JOURNAL OF Materials CHEMISTRY

# Structure and electrical properties of oxygen-deficient hexagonal $BaTiO_3$

**Derek C. Sinclair,[a]† Janet M. S. Skakle,[a] Finlay D. Morrison,[a]† Ronald I. Smith[b] and Tim P. Beales[c]**

[a]*Chemistry Department, University of Aberdeen, Meston Walk, UK AB24 3UE*
[b]*Rutherford Appleton Laboratory, Chilton, Didcot, UK OX11 0QX*
[c]*Centre for Superconducting and Electronic Materials, University of Wollongong, NSW 2522, Australia*

***Received 4th February 1999, Accepted 30th March 1999***

Rietveld refinements using neutron diffraction data have been used to determine the crystal structure of a series of oxygen-deficient barium titanate powders, $BaTi^{IV}_{1-x}Ti^{III}_{x}O_{3-x/2}$ ($0<x<0.30$). The powders were prepared by reduction of stoichiometric, tetragonal $BaTiO_3$ in a vacuum furnace at temperatures above 1300 °C and under an oxygen partial pressure of 0.1 mbar. The 6H-$BaTiO_3$ hexagonal perovskite structure is retained throughout and partial reduction of $Ti^{IV}$ to $Ti^{III}$ is accompanied by the formation of O(1) oxygen vacancies in the h-$BaO_3$ layers which separate pairs of occupied face-sharing octahedra, $Ti_2O_9$. There is no evidence of O(2) vacancies associated with corner sharing $TiO_6$ octahedra. The Ti(2)–Ti(2) separation within face sharing dimers increases from 2.690(4) Å for $x=0$ to 2.7469(30) Å for $x=0.30$. $BaTiO_{2.85}$ is a band-gap semiconductor at 300 K with a resistivity of *ca.* 1 Ω cm and activation energy 0.16 eV. A switch in conduction mechanism to variable range hopping (VRH) of electrons between $Ti^{III}$ and $Ti^{IV}$ ions occurs on cooling below 240 K.

## Introduction

Ferroelectric $BaTiO_3$-based ceramics find applications in capacitors, thermistors and piezo-electric devices, and form the cornerstone of the electroceramics market. Although the electrical properties of tetragonal $BaTiO_3$ (t-$BaTiO_3$) and doped-$BaTiO_3$ have been widely studied, their defect chemistry is complex and poorly understood.[1] In addition, very little is known about the high temperature, 6H-hexagonal polymorph (h-$BaTiO_3$) which exists only at temperatures >1460 °C for undoped samples prepared in air.[2] There are no reports on the crystal chemistry and very few on the physical properties[3–6] of oxygen-deficient h-$BaTiO_3$, *i.e.* $BaTi^{IV}_{1-x}Ti^{III}_{x}O_{3-x/2}$. To our knowledge, the solid solution limit and distribution of oxygen vacancies have not been established. There is general agreement, however, that the crystal symmetry at room temperature changes from tetragonal- to cubic-perovskite for small values of $x$, *ca.* $<0.03$ before transforming to the hexagonal, 6H-perovskite for $x>0.03$.

The crystal structures of many barium titanates including h-$BaTiO_3$, $Ba_6Ti_{17}O_{40}$, $Ba_4Ti_{13}O_{30}$, $Ba_2Ti_9O_{20}$ and $BaTi_5O_{11}$ can be described as hexagonal close packing of Ba and O atoms with partial occupancy of octahedral sites by Ti.[7] In a single crystal X-ray study, Akimoto *et al.*[8] reported the structure of stoichiometric ($x=0$), h-$BaTiO_3$ in space group $P6_3/mmc$ in terms of close packed $BaO_3$ layers, with a $[cch]_2$ sequence, *i.e.* $[Ba(2)O(2)_3Ba(2)O(2)_3Ba(1)O(1)_3]_2$. Atoms Ti(1) and Ti(2) occupy corner- and face-sharing octahedra, respectively, (Fig. 1) with rather short Ti(2)–Ti(2) distances in the face-sharing $Ti_2O_9$ octahedra. Stoichiometric h-$BaTiO_3$ has been reported to undergo structural phase transitions at 220 and 78 K,[4] and Zandbergen and Ijdo[9] have shown that octahedral tilting around the threefold axes in 6H-perovskites can produce 'distorted' 6H-$BaTiO_3$-type structures with lower symmetry (space group $P6_3/m$) and axial ($c/a$) ratios >2.45 (6), the theoretical value expected for the 'undistorted' 6H-$BaTiO_3$ structure.

†New Address: Department of Engineering Materials, University of Sheffield, Mappin Street, UK S1 3JD.

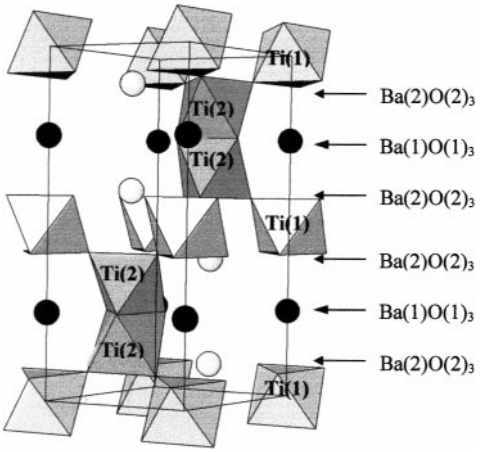


**Fig. 1** The crystal structure of 6H-$BaTiO_3$.

Despite extensive literature on the crystal chemistry of stoichiometric and oxygen-deficient 6H-perovskites containing Ba on the A-site and a variety of transition metals, *e.g.* Cr, Mn, Fe, Co on the B-site[10–15] few reports exist on Ti-based systems.[16,17] Recently, Grey *et al.*[17] reported a series of h-$Ba(Ti,Fe)O_{3-\delta}$ materials where $Ti^{IV}$ was progressively replaced by $Fe^{III}$ and/or $Fe^{IV}$ with oxygen vacancies being formed exclusively in O(1) sites within the h-$BaO_3$ layers. In their study, the largest variation in atomic distances for 6H-$BaMO_{3-\delta}$ where M=(Ti,Fe) was associated with pairs of M(2) atoms and/or Ba(2) atoms as opposed to M–O distances. This led the authors to rationalise structural variations in terms of Ba and M atom packing as oxygen was removed from O(1) sites.

Removal of O(1) results in increased repulsion between M(2) atoms within face sharing octahedra and hence to a lengthening of the Ti(2)–Ti(2) distance. In addition, distance Ba(2)–M(2) remained unchanged, resulting in longer Ba(2)–Ba′(2) and shorter Ba(2)–M′(2) distances. The Ba(2)–M(2) distance was proposed to remain constant at the value of 3.40 Å reported for stoichiometric 6H-$BaTiO_3$[8] which

is shorter than that calculated for BaTi alloy, 3.58 Å,[17] and, therefore, was unlikely to contract any further. A decrease in Ba(2)–M′(2) was suggested to be plausible as the reported distance of 3.50 in 6H-$BaTiO_3$ is *ca.* 0.1 Å longer than Ba(2)–M(2).

Here, we report Rietveld refinements of the structures of a series of oxygen-deficient h-$BaTiO_3$ (h-$BaTiO_{3-x/2}$) powders prepared at 1300–1510 °C, and low oxygen partial pressure, $p(O)_2$ *ca.* 0.1 mbar, using powder neutron diffraction data. The 6H-perovskite structure is retained throughout and reduction is accompanied by the formation of O(1) vacancies in the h-$BaO_3$ layers. Electrical resistivity, ($\rho$) data in the range 30–300 K are reported for $BaTiO_{2.85}$ ($x=0.30$).

## Experimental

h-$BaTiO_{3-x/2}$ samples were prepared by heating high purity (99.999%) t-$BaTiO_3$ powder in a Torvac, graphite vacuum furnace (Series 10, Model VI). Batches (4–5 g) of t-$BaTiO_3$ powder were placed on a carbon felt boat and accurately weighed before heating to 1300, 1370, 1440 or 1510 °C for 10 h under $p(O_2)$ of 0.1 mbar. Samples fired above 1510 °C melted whereas those fired below 1300 °C retained tetragonal or cubic symmetry. After initial firing, the blue/black powders were removed from the furnace, weighed, reground in acetone using an agate mortar and pestle and reweighed in the carbon boat prior to refiring. Experience showed the regrinding–refiring schedule had to be repeated four times to obtain a constant weight and therefore, for powders to achieve equilibrium. In an attempt to prepare stoichiometric h-$BaTiO_3$, 3–4 g of a sample prepared in vacuum at 1440 °C was re-oxidised in air at 650 °C for 24 h.

Time-of-flight powder neutron diffraction (ND) data were collected on the POLARIS diffractometer at the UK spallation neutron source, ISIS, Rutherford Appleton Laboratory, using cylindrical vanadium containers. The crystal structures were refined by the Rietveld method with the program TF14LS[18,19] using data collected over the time-of-flight range 2000–19500 μs in the highest resolution, backscattering detectors. Neutron scattering lengths of 5.07(3), −3.438(2) and 5.803(4) fm were assigned to Ba, Ti and O, respectively.[20] Observed peak shapes were modelled using a convolution of a Voigt and two exponential decay functions. Conventional four-terminal dc electrical resistivity measurements were carried out on small rectangular bars cut from sintered pellets. The resistivity was measured from 30 to 300 K at a constant current of 1 mA using Ag paste electrodes.

## Results and discussion

All ND patterns were fully indexed on the 6H-$BaTiO_3$ pattern[8] except for the sample prepared at 1510 °C which contained several additional weak reflections associated with an impurity phase. These extra reflections were omitted from the Rietveld refinement of this sample. Initially, all coordinates were set to reported values and site occupancies were freely refined using starting parameters of h-$BaTiO_3$, space group $P6_3/mmc$.[8] The refinements showed that all sites except O(1) were fully occupied, within a few estimated standard deviations (esds). Next, all cation site occupancies were fixed to unity, all isotropic temperature factors ($B_{iso}$) were freely refined and the site occupancies of the oxygen atoms refined; again, O(2) refined to full occupancy. Thus, in the final refinements, all sites except O(1) were constrained to be fully occupied. Final values from the Rietveld refinements for the reduced and re-oxidised h-$BaTiO_{3-x/2}$ powders, along with literature data[8] are given in Table 1.

The crystallographic model produced good refinements for the single phase samples, with all $R_{wp}<3.2\%$ and a respectable refinement with $R_{wp}<6\%$ for the phase mixture prepared at 1510 °C. The results clearly demonstrate that oxygen is removed from the O(1) sites. There was no evidence of oxygen vacancies in O(2) sites within the cubic close packed layers. The oxygen contents were calculated from the sum of the O site occupancies; the fraction of $Ti^{III}$ ($x$ value) was estimated from the general formula $BaTi^{IV}_{1-x}Ti^{III}_{x}O_{3-x/2}$. At the lower limit of the solid solution ($x=0.33$), the average composition of the hexagonal close packed layers approaches a value of $BaO_{2.50}$. Selected area electron diffraction on h-$BaTiO_{3-x/2}$ powders did not show evidence of any supercell, suggesting a

**Table 1** Final refined parameters, oxygen occupancies and oxygen content for h-$BaTi^{IV}_{1-x}Ti^{III}_{x}O_{3-x/2}$

| Sample | Single crystal[8] | Re-oxidised (650 °C/air) | Reduced (1300 °C/0.1 mbar) | Reduced (1370 °C/0.1 mbar) | Reduced (1440 °C/0.1 mbar) | Reduced[a] (1510 °C/0.1 mbar) |
|---|---|---|---|---|---|---|
| $R_p$ (%) | 3.7[b] | 4.99 | 3.27 | 3.62 | 4.61 | 7.20 |
| $R_{wp}$ (%) | 3.6[c] | 3.14 | 2.09 | 2.37 | 3.20 | 5.29 |
| $a$/Å | 5.7238(7) | 5.725371(6) | 5.731160(6) | 5.736580(6) | 5.738890(6) | 5.738300(7) |
| $c$/Å | 13.9649(9) | 13.97005(6) | 13.99109(6) | 14.01046(5) | 14.02040(7) | 14.01938(6) |
| Ba(2) (4f)[d] | | | | | | |
| $z$ | 0.09671(5) | 0.09733(8) | 0.09649(7) | 0.09615(7) | 0.09627(10) | 0.09707(17) |
| Ti(2) (4f)[e] | | | | | | |
| $z$ | 0.84633(14) | 0.84646(13) | 0.84733(10) | 0.84794(11) | 0.84796(15) | 0.8477(2) |
| O(1) (6h)[f] | | | | | | |
| $x$ | 0.5185(6) | 0.51735(8) | 0.51741(7) | 0.51749(8) | 0.51739(12) | 0.51753(2) |
| $y$ | 0.0370 | 0.03475(15) | 0.03486(14) | 0.03504(17) | 0.03478(23) | 0.0351(4) |
| O(2) (12k)[g] | | | | | | |
| $x$ | 0.8349(6) | 0.83464(8) | 0.83426(7) | 0.83400(7) | 0.83383(10) | 0.83388(17) |
| $y$ | 0.6698 | 0.66929(15) | 0.66854(13) | 0.66798(14) | 0.66770(19) | 0.6678(3) |
| $z$ | 0.0802(2) | 0.08040(4) | 0.08076(3) | 0.08094(3) | 0.08100(4) | 0.08086(7) |
| $B_{iso}$/Å$^2$ | | | | | | |
| Ba(1) | 0.43 | 0.271(17) | 0.358(15) | 0.420(17) | 0.45(2) | 0.45(4) |
| Ba(2) | 0.52 | 0.282(12) | 0.369(11) | 0.384(11) | 0.380(15) | 0.31(2) |
| Ti(1) | 0.67 | 0.52(3) | 0.54(2) | 0.512(2) | 0.50(3) | 0.52(5) |
| Ti(2) | 0.62 | 0.372(17) | 0.417(14) | 0.457(16) | 0.44(2) | 0.37(3) |
| O(1) | 0.65 | 0.233(13) | 0.368(12) | 0.416(14) | 0.401(19) | 0.29(3) |
| O(2) | 0.66 | 0.339(6) | 0.404(5) | 0.419(5) | 0.418(7) | 0.363(11) |
| O(1) Site occupancy | 1.0 | 0.969(5) | 0.916(4) | 0.879(4) | 0.848(6) | 0.827(10) |
| Composition | $BaTiO_3$ | $BaTiO_{2.97}$ | $BaTiO_{2.92}$ | $BaTiO_{2.88}$ | $BaTiO_{2.85}$ | $BaTiO_{2.83}$ |
| Fraction of $Ti^{III}$, $x$ | 0.00 | 0.06 | 0.16 | 0.24 | 0.30 | 0.34 |

[a]Sample was a phase mixture, see text for details. [b]$R$ (%) not $R_p$. [c]$wR$ (%) not $R_{wp}$. [d]Ba(2) (1/3,2/3,$z$). [e]Ti(2) (1/3,2/3,$z$). [f]O(1) ($x$,$y$,1/4). [g]O(2) ($x$,$y$,$z$).

random distribution of O(1) vacancies within the h-$BaO_{3-x/2}$ layers.

The variation in unit cell parameters as a function of $x$ is shown in Fig. 2. A smooth expansion in both $a$ and $c$ is observed as oxygen is removed from the O(1) sites. The value of $x$ for the single crystal data (open symbols) is assumed to be zero, as no O site occupancies were reported.[8] Refined unit cell parameters for the phase mixture containing $BaTiO_{2.83}$ are close to those for $BaTiO_{2.85}$, suggesting the lower oxygen limit in reduced h-$BaTiO_{3-x/2}$ to be *ca.* 2.83–2.85, corresponding to a $Ti^{III}$ content of *ca.* 30–33%. This limit appears reasonable given that several 6H-perovskites of general formula $Ba(M_{1/3}Ti_{2/3})O_{3-\delta}$ ($M^{III}$=Mn, Fe, Co, Ru, Rh or Ir) have been reported.[21]

This limit of $x \approx 0.30$ is much higher than that reported by Arend and Kihlborg[22] who prepared h-$BaTiO_{2.977}$ by reducing t-$BaTiO_3$ in a flow of $H_2$ at 1500 °C for 5 h. Their $Ti^{III}$ content was determined *via* colorimetry. Their lattice parameters, $a$= 5.7257(3) and $c$=13.9679(8) Å for $BaTiO_{2.977}$, are in excellent agreement with those interpolated from Fig. 2, and further support the validity of using ND to determine oxygen contents in h-$BaTiO_{3-x/2}$ powders. In an earlier study, Dickson *et al.*[21] suggested a solid solution limit of $x$=0.40, corresponding to $BaTiO_{2.80}$. A sample of nominal composition $x$=0.48 was prepared *in vacuo* from appropriate mixtures of $BaCO_3$, Ti metal, $Ti_2O_3$ and $TiO_2$. No details of the product purity were provided. Lattice parameters of $a$=5.74 and $c$=14.1 Å are in reasonable agreement with our results for $a$ for the solid solution limit, but there is a significant discrepancy in the value of $c$. In their sample, the $Ti^{III}$ content was determined by the weight gained by the product on re-oxidation to h-$BaTiO_3$ in air.

Our results are in good agreement with existing literature on oxygen-deficient 6H-perovskites. Jacobson[23] demonstrated an unequal distribution of oxygen vacancies between h-$BaO(1)_3$ and c-$BaO(2)_3$ layers in 6H-$BaFeO_{2.79}$. Most vacancies were located in hexagonal layers with average composition $BaO(1)_{2.50}$ whereas the cubic layers had an average composition of $BaO(2)_{2.835}$. Grey *et al.*[17] reported that oxygen vacancies formed exclusively in O(1) sites within the h-$BaO_3$ layers in h-$Ba(Ti,Fe)O_{3-\delta}$, again consistent with our results for h-$BaTiO_{3-x/2}$.

Selected metal–metal bond distances for h-$BaTiO_{3-x/2}$ samples are shown in Fig. 3. The major structural change with increasing $x$ is the increase in Ti(2)–Ti(2) distance within the face-sharing octahedra from 2.690(4) to 2.7394(40) Å, [Fig. 3(a)]. These values are consistent with other mixed $Ti^{III}/Ti^{IV}$ barium titanates containing face-sharing $TiO_6$ octahedra, *e.g.* 2.730(2) Å for $Ba_2Ti_{13}O_{22}$[24] and are also intermediate between those observed for $Ti^{III}$ and mixed

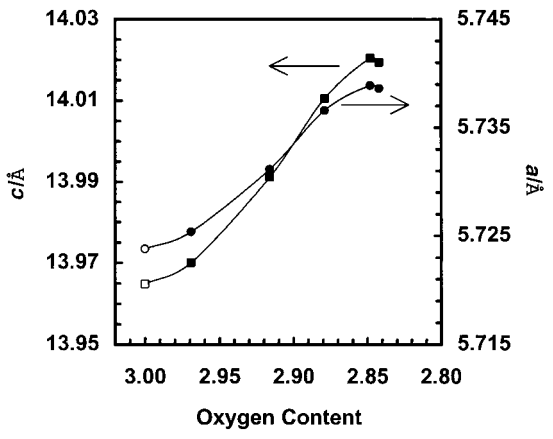


**Fig. 2** Cell parameters *versus* oxygen content for h-$BaTiO_{3-x/2}$. Filled circles and squares represent $a$ and $c$ data, respectively. Open symbols are for 6H-$BaTiO_3$ from Akimoto *et al.*[8]

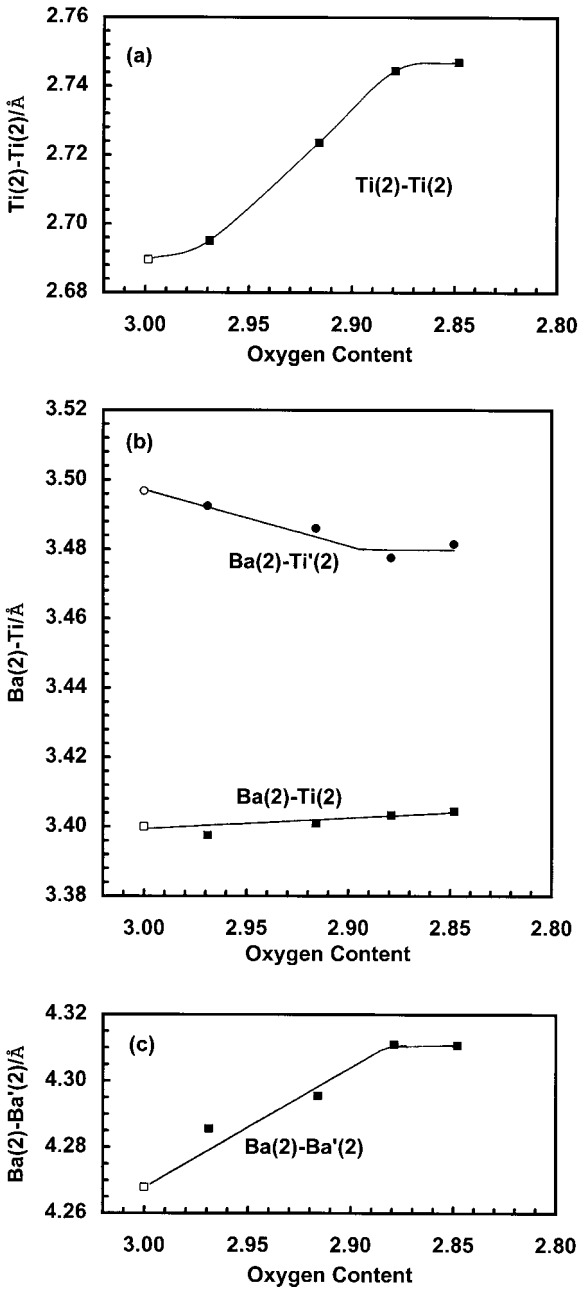


**Fig. 3** Selected M–M distances as a function of oxygen content for h-$BaTiO_{3-\delta}$ (filled circles). Open squares are for 6H-$BaTiO_3$ from Akimoto *et al.*[8]

$Ti^{III}/Ti^{IV}$ oxides, *e.g.* 2.579 Å for $Ti_2O_3$[25] and 2.811 Å for $Ti_4O_7$.[26] The Ba(2)–Ti(2) distance remains close to 3.40 Å for all values of $x$, whereas Ba(2)–Ti′(2) decreases from 3.50 to 3.48 Å with increasing $x$ [Fig. 3(b)]. As a result, Ba(2)–Ba′(2) increases from 4.28 to 4.31 Å [Fig. 3(c)]. These variations are in good agreement with the model proposed by Grey *et al.*[17] for h-$Ba(Ti,Fe)O_{3-\delta}$.

With increasing $x$, the Ti(1)–O(2) distance increases from 1.983(5) to 2.0043(8) Å as does Ti(2)–O(1), from 1.992(4) to 2.0219(16) Å, but Ti(2)–O(2) decreases smoothly from 1.958(5) to 1.9374(14) Å (Fig. 4). Average Ti–O distances for h-$BaTiO_3$ and $BaTiO_{2.85}$ are 1.983(5) and 2.0043(8) Å for Ti(1), and 1.975(5) and 1.9797(14) Å for Ti(2), respectively. The average Ti(2)–O distance remains constant at *ca.* 1.98 Å for all values of $x$, Fig. 4, and is close to the mean distance of 1.976 Å calculated from a survey of 58 octahedral $Ti^{IV}$–O distances in 10 different barium titanates.[7] The short Ti(2)–O(2) distance of 1.9374(14) Å for $BaTiO_{2.85}$ is comparable to the shortest $Ti^{IV}$–O bond length reported in the survey.

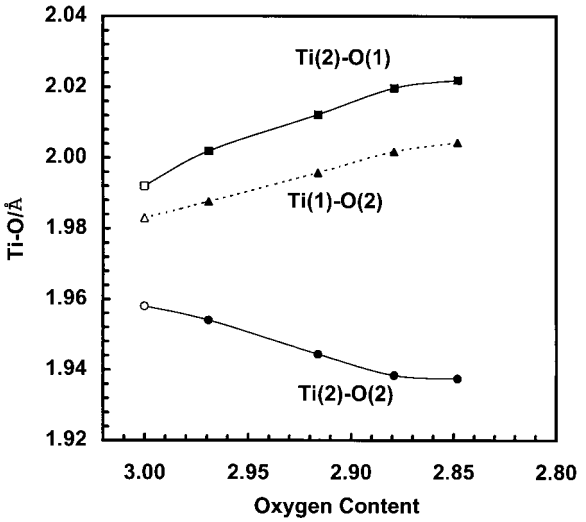


**Fig. 4** Selected Ti–O bond lengths as a function of oxygen content for h-$BaTiO_{3-\delta}$ (filled circles). Open symbols are for 6H-$BaTiO_3$ from Akimoto *et al.*[8]

In contrast, the mean Ti(1)–O distance increases with $x$ and the value of 2.0043(8) Å for $BaTiO_{2.85}$ is intermediate between those of 2.048 Å for $Ti^{III}$–O in $Ti_2O_3$[25] and 1.976 Å for $Ti^{IV}$–O.[7] Although a random distribution of $Ti^{III}$ and $Ti^{IV}$ ions across Ti(1) and Ti(2) sites cannot be excluded, bond length calculations suggest that $Ti^{III}$ ions are more likely to be located on Ti(1) as opposed to Ti(2) sites.

ND data for $BaTiO_{2.85}$ at 4 K did not reveal any change in crystal symmetry. The data refined on the 'undistorted' 6H-$BaTiO_3$ crystallographic model with lattice parameters of $a=5.723140(5)$ and $c=13.95614(5)$ Å and $R_{wp}=1.95\%$. The axial ratio at 4 and 300 K was 2.44, which is close to the theoretical value of 2.45 expected for the 'undistorted' 6H-$BaTiO_3$ structure.

Resistivity data for a polycrystalline sample of $BaTiO_{2.85}$ in the temperature range *ca.* 30–300 K are shown in the form of an Arrhenius plot (Fig. 5). Arrhenius-type behaviour with an activation energy of *ca.* 0.16 eV can be observed in the limited range 240–300 K where $\rho<1\ \Omega$ cm (Fig. 5, inset). This suggests a band-type model may be appropriate where oxygen vacancies form donor states *ca.* 0.1–0.2 eV below the conduction band. This model is commonly used to explain room

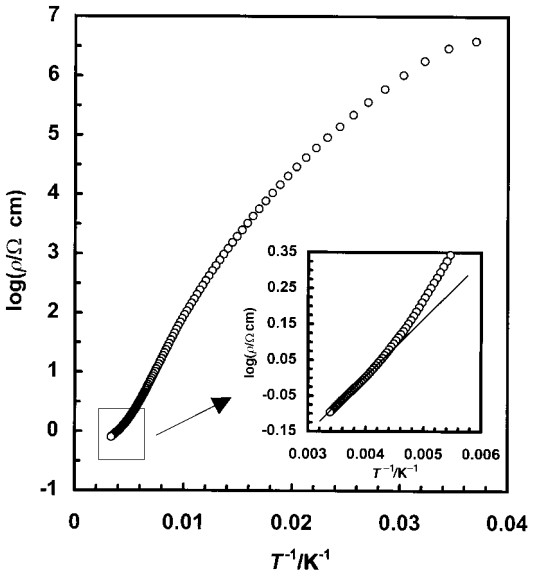


**Fig. 5** $\log(\rho/\Omega\,\mathrm{cm})$ *versus* reciprocal temperature for $BaTiO_{2.88}$. Inset shows $\log(\rho)$ for the range *ca.* 160–330 K on an expanded scale.

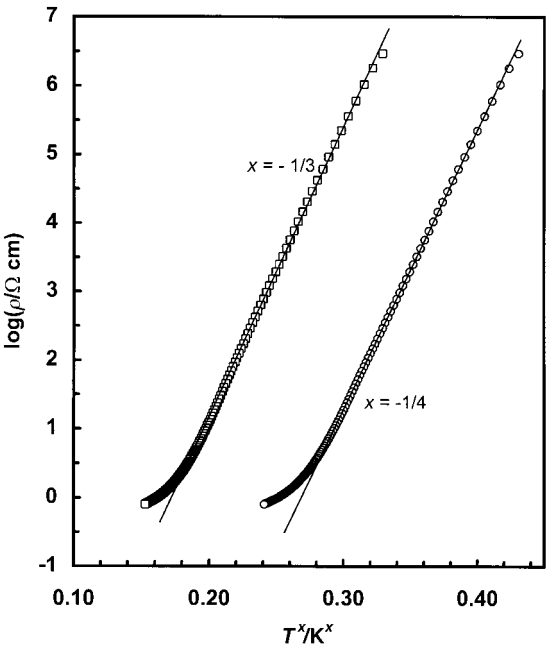


**Fig. 6** $\log(\rho/\Omega\,\mathrm{cm})$ *versus* $T^x$ for $BaTiO_{2.88}$ where $x=-1/3$ (open squares) and $-1/4$ (open circles).

temperature semiconductivity in oxygen-deficient t-$BaTiO_3$[27] and may also be appropriate for h-$BaTiO_{3-x/2}$.

Values of $\rho$ increase by several orders of magnitude below *ca.* 160 K and pronounced curvature occurs in the Arrhenius plot. Similar behaviour has been observed for a variety of transition metal containing 6H-perovskites, for example $Ba_2(Co,Ru)O_6$[28] and $Ba_3(Fe,Ru_2)O_9$.[29] Such behaviour is normally explained as variable range hopping (VRH) based on the Mott–Davis VRH law where $\log(\rho)$ shows a linear dependence on $T^{-1/3}$ or $T^{-1/4}$ for two and three dimensional hopping, respectively.[30] Plots of $\log(\rho)$ *vs.* $T^{-1/3}$ and $T^{-1/4}$ for h-$BaTiO_{2.85}$ are shown in Fig. 6, where solid lines are least-square fits of the data below 160 K to the Mott–Davis VRH law and have correlation coefficients of 0.9996 and 0.9999, respectively. Although $T^{-1/4}$ appears to give a better fit at low temperatures, the dimensionality of the hopping process is indistinguishable owing to the high correlation coefficients associated with the fitted data.

In the 'undistorted' 6H-$BaTiO_3$ crystal structure,[8] each $Ti(2)_2O_9$ dimer is connected to six $Ti(1)O_6$ octahedra. In addition to the strong overlap of d-orbitals between Ti(2) ions within the dimers it is plausible that good overlap of d-orbitals also exists between Ti(1) and Ti(2) ions. This may favour a three-dimensional hopping process, however, band structure calculations and electrical measurements on single crystals where $\rho$ can be measured as a function of crystal orientation are required before the dimensionality of VRH in h-$BaTiO_{3-x/2}$ at low temperatures is established.

As the ND pattern of $BaTiO_{2.88}$ at 4 K did not show evidence of any modification from the 'undistorted' 6H-$BaTiO_3$ structure obtained at 300 K, the change in transport mechanism, which occurs over a rather broad temperature range, *ca.* 160–240 K, appears to be associated with an electronic as opposed to a structural phase transition. There may, however, be subtle tilting of the octahedra which has not been detected by ND. Further structural, electrical and magnetic measurements are in progress to fully characterise the composition–property relationships in h-$BaTiO_{3-x/2}$ materials.

## Conclusions

The 6H-perovskite structure reported for stoichiometric h-$BaTiO_3$ is retained throughout the h-$BaTiO_{3-x/2}$ series.

Reduction is accompanied by the formation of O(1) vacancies in the h-$BaO_3$ layers and changes in unit cell dimensions are dominated by an increase in Ti(2)–Ti(2) separation within face sharing dimers. Such changes are consistent with increasing Coulombic repulsion between adjacent Ti(2) ions as oxygen ions are removed from the shared octahedral faces. The end member of the solid solution, $BaTiO_{2.85}$, is semiconducting with $\rho \approx 1\ \Omega$ cm at 300 K, however, $\rho$ rises dramatically below *ca.* 160 K where data are consistent with models based on variable range hopping of electrons between $Ti^{III}$ and $Ti^{IV}$ ions.

## Acknowledgements

We would like to thank Dr E. E. Lachowski for selected area electron diffraction measurements and Professor A.R West for useful discussions.

## References

1 J. Nowotny and M. Sloma, *Solid State Ionics*, 1991, **49**, 129.
2 R. M. Glaister and H. F. Kay, *Proc. Phys. Soc. LXXVI*, 1960, **5**, 763.
3 Y. Akishigue, T. Atake, Y. Saito and E. Sawaguchi, *J. Phys. Soc. Jpn.*, 1988, **57**, 718.
4 Y. Akishigue, G. Oomi, T. Yamamoto and E. Sawaguchi, *J. Phys. Soc. Jpn*., 1989, **58**, 930.
5 E. Buixaderas, S. Kamba, J. Petzelt, M. Wada, A. Yamanaka and K. Inoue, *J. Korean Phys. Soc*., 1998, **32**, S578.
6 Y. Akishigue, Y. Yamazaki, T. Nakanishi and N. Mori, *J. Korean Phys. Soc*., 1998, **32**, S386.
7 E. Tillmanns, W. Hofmeister and W. H. Baur, *J. Solid State Chem.*, 1985, **58**, 14.
8 J. Akimoto, Y. Gotoh and Y. Oosawa, *Acta. Crystallogr.*, *Sect. C*, 1994, **50**, 160.
9 H. W. Zandbergen and D. J. W. Ijdo, *Acta Crystallogr.*, *Sect. C*, 1984, **40**, 919.
10 F. K. Patterson, C. W. Moeller and R. Ward, *Inorg. Chem*., 1963, **2**, 196.
11 G. Blasse, *J. Inorg. Nucl. Chem*., 1965, **27**, 993.
12 P. C. Donohue, L. Katz and R. Ward, *Inorg. Chem*., 1966, **5**, 335.
13 J. M. Longo and J. A. Kafalas, *J. Solid State Chem.*, 1969, **1**, 103.
14 T. Negas and R. S. Roth, *J. Solid State Chem.*, 1971, **3**, 323.
15 B. L. Chamberland, *J. Solid State Chem*., 1983, **48**, 318.
16 D. Verdoes, H. W. Zandbergen and D. J. W. Ijodo, *Acta Crystallogr.*, *Sect. C*, 1985, **41**, 170.
17 I. E Grey, C. Li, L. M. D. Cranswick, R. S. Roth and T. A. Vanderah, *J. Solid State Chem.*, 1988, **135**, 312.
18 R. I. Smith and S. Hull, Report RAL-TR-97–038, Rutherford Appleton Laboratory, 1997.
19 W. I. F. David, R. M. Ibberson and J. C. Matthewmann, Report RAL-92–032, Rutherford Appleton Laboratory, 1992.
20 V. F. Sears, *Neutron News*, 1992, **3**, 26.
21 J. G. Dickson, L. Katz and R. Ward, *J. Am. Chem. Soc*., 1961, **83**, 3026.
22 H. Arend and L. Kihlborg, *J. Am. Ceram. Soc.*, 1969, **52**, 63.
23 A. J. Jacobson, *Acta Crystallogr.*, *Sect. B*, 1976, **32**, 1087.
24 J. Akimoto, Y. Gotoh, M. Kawaguchi and Y. Oosawa, *J. Solid State Chem*., 1994, **113**, 384.
25 W. R. Robinson, *J. Solid State Chem*., 1974, **9**, 255.
26 M. Marezio, D. B. McWahn, P. D. Dernier and J. P. Remeika, *J. Solid State Chem.*, 1973, **6**, 213.
27 A. M. J. H. Seuter, *Philips Res. Rep. Suppl.*, 1974, **3**, 1.
28 S. H. Kim and P. D. Battle, *J. Solid State Chem.*, 1995, **114**, 174.
29 J. T. Rijssenbeek, P. Matl, B. Batlogg, N. P. Ong and R. J. Cava, *Phys. Rev. B*, 1998, **58**, 10315.
30 N. F. Mott and E. A. Davis, *Electronic Processes in Non-Crystalline Materials*, Oxford University Press, London, 2nd edn., 1979.

*Paper 9/00957D*